

# Chemical Science

Accepted Manuscript



This is an *Accepted Manuscript*, which has been through the Royal Society of Chemistry peer review process and has been accepted for publication.

*Accepted Manuscripts* are published online shortly after acceptance, before technical editing, formatting and proof reading. Using this free service, authors can make their results available to the community, in citable form, before we publish the edited article. We will replace this *Accepted Manuscript* with the edited and formatted *Advance Article* as soon as it is available.

You can find more information about *Accepted Manuscripts* in the [Information for Authors](#).

Please note that technical editing may introduce minor changes to the text and/or graphics, which may alter content. The journal's standard [Terms & Conditions](#) and the [Ethical guidelines](#) still apply. In no event shall the Royal Society of Chemistry be held responsible for any errors or omissions in this *Accepted Manuscript* or any consequences arising from the use of any information it contains.

## EDGE ARTICLE

# Tunable Electrical Conductivity in Oriented Thin Films of Tetrathiafulvalene-Based Covalent Organic Framework

Cite this: DOI: 10.1039/x0xx00000x

Received 00th January 2012,  
Accepted 00th January 2012

DOI: 10.1039/x0xx00000x

www.rsc.org/

Song-Liang Cai,<sup>†ab</sup> Yue-Biao Zhang,<sup>†cd</sup> Andrew B. Pun,<sup>a</sup> Bo He,<sup>a</sup> Jinhui Yang,<sup>de</sup> Francesca M. Toma,<sup>ef</sup> Ian D. Sharp,<sup>eg</sup> Omar M. Yaghi,<sup>cd</sup> Jun Fan,<sup>b</sup> Sheng-Run Zheng,<sup>b</sup> Wei-Guang Zhang<sup>b\*</sup> and Yi Liu<sup>a\*</sup>

Despite the high charge-carrier mobility in covalent organic frameworks (COFs), the low intrinsic conductivity and poor solution processability still impose a great challenge for their applications in flexible electronics. We report the growth of oriented thin films of a tetrathiafulvalene-based COF (TTF-COF) and its tunable doping. The porous structure of the crystalline TTF-COF thin film allows the diffusion of dopants such as I<sub>2</sub> and tetracyanoquinodimethane (TCNQ) for redox reactions, while the closely packed 2D grid sheets facilitate the cross-layer delocalization of thus-formed TTF radical cations to generate more conductive mixed-valence TTF species, as is verified by UV-Vis-NIR and electron paramagnetic resonance spectra. Conductivity as high as 0.28 S/m is observed for the doped COF thin films, which is three orders of magnitude higher than that of the pristine film and is among the highest for COF materials.

## Introduction

Electroactive organic materials, with charge-transfer molecular crystals<sup>1</sup> and conjugated polymers<sup>2</sup> being the most representative classes, have garnered much attention for their potential applications in flexible electronics.<sup>3</sup> Two-dimensional (2D) covalent organic frameworks (COFs),<sup>4</sup> which contain periodic structure within a 2D sheet and columnar alignment in the third dimension, are a class of lightweight porous materials that combine both the long-range order feature of molecular crystals and the extended conjugation as in conjugated polymers. With the additional feature of permanent porosity, COFs emerge as a very promising kind of electroactive organic material.<sup>5</sup> COFs containing  $\pi$ -electron rich or deficient units, such as thiophene,<sup>6</sup> pyrene,<sup>7</sup> phthalocyanine,<sup>8</sup> porphyrine,<sup>9</sup> squaraine,<sup>10</sup> rylene diimide,<sup>11</sup> benzothiadiazole,<sup>12</sup> and 2,6-diaminoanthraquinone<sup>13</sup> have been prepared, some of which are shown to have high spectroscopic carrier mobilities by electrodeless microwave conductivity measurements.<sup>8a,8b,9,11a,12</sup> The real electrical performance in a wired circuit, however, still remains low on account of the intrinsically low carrier concentrations in organic materials, as well as the lack of solution processability of powdery COF that impedes their integration into devices.<sup>14</sup> Growth of crystalline COF thin films on substrates is highly advantageous for device fabrication.

Recently on-surface growth of COF has been demonstrated to form preferentially oriented columnar stacks<sup>11b,15</sup> or single layers.<sup>16</sup> On the other hand, the low intrinsic electrical conductivity can be remedied by chemical doping methods which has been applied on organic semiconductors.<sup>2a</sup> Combining the thin film growth and chemical doping, a recent study on metal-organic frameworks (MOFs) has shown enhanced electrical conductivity up to six orders of magnitude.<sup>17</sup> However, a pure organic porous framework material that can satisfy both easy thin film growth and chemical doping remains unprecedented.

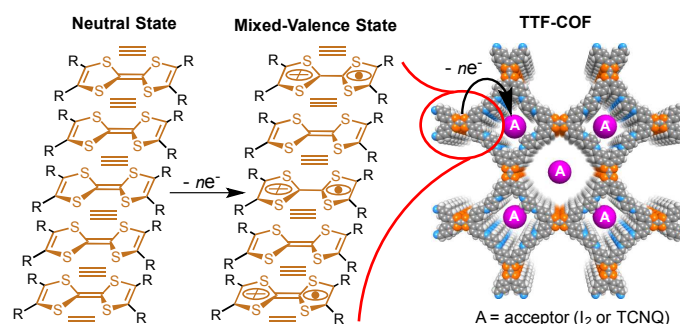
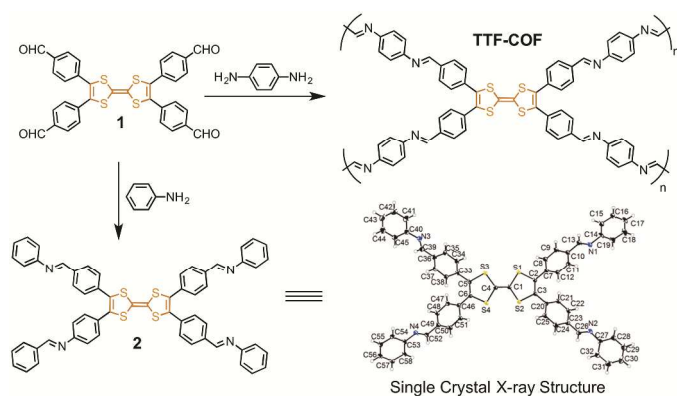


**Figure 1.** Illustration of the mixed-valence state in TTF-COF. The “≡” indicates inter-TTF-layer interactions.

Tetrathiafulvalene (TTF) is an excellent electron donor that is known to form highly conductive charge-transfer crystals with electron acceptors such as I<sub>2</sub> or tetracyanoquinodimethane (TCNQ).<sup>1,18</sup> A well-defined 2D framework containing TTF units offers great opportunity for the particular alignment and stacking of TTF columns as conductive pathways.<sup>19</sup> Meanwhile, the open nanochannels within the 2D COFs allow the incorporation of molecular dopants as charge-transfer partner.<sup>6a</sup> The confluence of such structural features sets the stages for the generation of mixed-valence TTF stacks, an essential species for high conductivity (Figure 1). Here we report the synthesis and characterization of a crystalline TTF-COF in the form of both powder<sup>20</sup> and thin film. Corresponding thin film devices show much enhanced electronic conductivity upon doping with electron acceptors, which are correlated to the formation of paramagnetic mixed-valence TTF species that can only be produced in closely packed TTF lattices.

## Results and discussion



Scheme 1. Synthesis of TTF-COF and Its Molecular Analogue 2.

Synthesis of the TTF-COF was carried out by reacting the TTF tetraaldehyde **1**<sup>21</sup> with 1,4-diaminobenzene in a mixture of degassed aqueous acetic acid (3 M)/dioxane/mesitylene (1:5:5 v/v/v) at 120 °C for 3 days (Scheme 1). TTF-COF was isolated as deep purple solid in 52% yield after filtration and extensive solvent wash. A “monomeric” analogue tetraimino-TTF (**2**) was also synthesized from condensation between aniline and **1**. Both **1** and **2** were characterized by single-crystal X-ray analysis (Scheme 1 and Figure S1 in Electronic Supplementary Information, ESI). Elemental analysis of TTF-COF reveals a CHN composition that matches well with the theoretical value (Calcd. for C<sub>46</sub>H<sub>28</sub>N<sub>4</sub>S<sub>2</sub>: C, 72.22; H, 3.69; N, 7.32%. Found: C, 72.03; H, 3.73; N, 7.59%). The formation of imine linkage in TTF-COF was confirmed by Fourier-transform infrared (FTIR) and solid-state nuclear magnetic resonance (NMR) spectroscopy, which was compared against those of its molecular analogue **2**. The FTIR spectrum of TTF-COF (Figure S7) shows an imine stretching vibration band at 1620 cm<sup>-1</sup>, which is identical to that of **2**. A resonance at 1700 cm<sup>-1</sup> in the spectrum of TTF-COF occurs at the same position in the spectra of both **1** and molecular analogue **2**. Since **2** contains no

carbonyl group, this vibration is thus believed to be intrinsic to the tetra-aryl-TTF skeleton, which happens to overlap with the carbonyl vibration. <sup>13</sup>C cross-polarization magic-angle spinning (CP-MAS) solid state NMR spectrum confirms the full conversion of aldehyde groups to imine bonds by the absence of carbonyl groups in the range of 180-200 ppm, together with new peaks appearing at 157.8 ppm and 150.2 ppm (Figure S13). Scanning electron microscopy (SEM) indicates (Figure S14) the presence of parallelogram-shaped microcrystals with defined edges. The PXRD pattern of TTF-COF shows a strongest diffraction peak at 2θ = 3.65°, together with weaker peaks at 2θ = 2.57, 5.87, 7.45 and 9.53°, which match the proposed 2D COF structure (Figure 2a-c and Figure S15) with AA packing. The diffraction peaks can be ascribed to the (110), (100), (210), (220) and (320) facets, respectively. Based on this structure, Pawley refinement of the PXRD pattern confirms the peak assignment and indicated negligible difference from the observed PXRD pattern (Figure 2a). In contrast, another “eclipsed” packing model with the TTF units in the second sheet lying orthogonal to these in the first one does not fit well with the experimental PXRD pattern (Figure S15 and S16). Permanent porosity of TTF-COF is illustrated by the nitrogen adsorption isotherm at 77 K (Figure S19), which indicates a Type I adsorption isotherm with steep uptake of 240 cm<sup>3</sup>/g at P/P<sub>0</sub> = 0.1. The Brunauer–Emmett–Teller (BET) surface is 720 m<sup>2</sup>/g. Thermal stability of TTF-COF is examined by thermal gravimetric analysis (TGA), which shows no weight loss up to 360 °C (Figure S20).

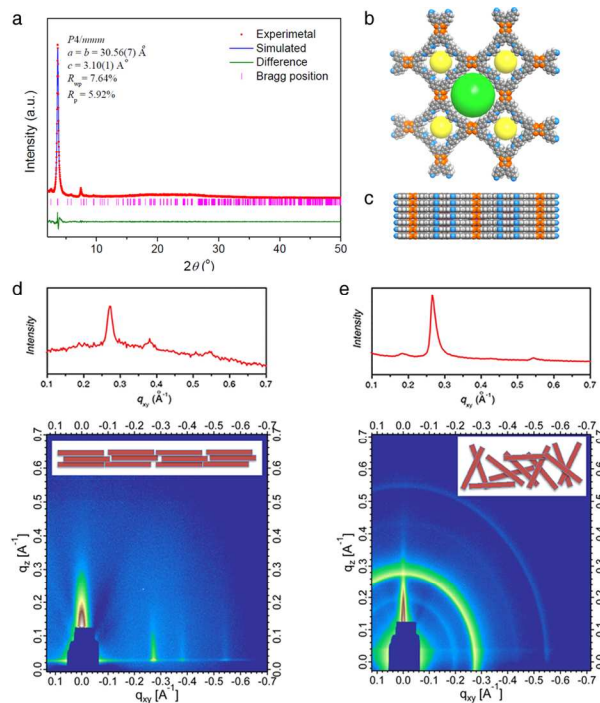
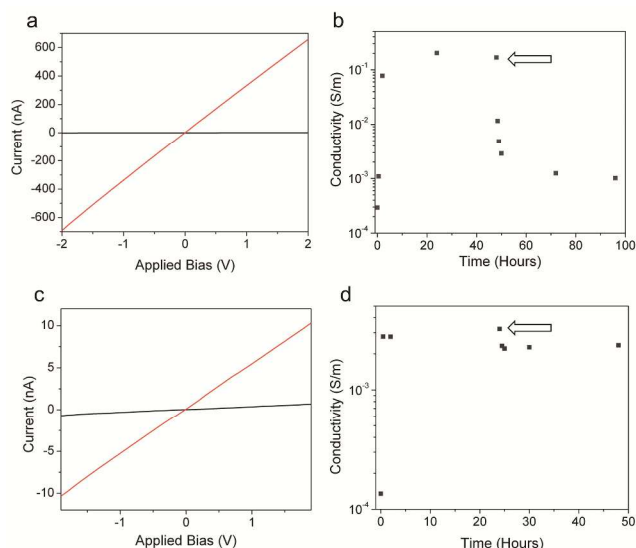


Figure 2. (a) Experimental and simulated PXRD patterns of TTF-COF. (b) Top and (c) side view of 2D TTF-COF with AA packing. GIWAXS and the in-plane diffraction patterns of (d) thin-film grown on substrate and (e) powder. Inset: cartoon showing the preferential (d) and random orientation (e) of crystallites in thin film and powder.

Thin films of TTF-COF with nominal thickness around 150 nm were grown *in situ* from the liquid phase on Si/SiO<sub>2</sub> substrates and transparent ITO-coated glass. Grazing incidence wide angle X-ray scattering (GIWAXS) of the thin films indicates (Figure 2d) their polycrystalline nature with preferential orientation of the columns normal to the substrate. In contrast, the bulk powder TTF-COF is also polycrystalline but only consists of randomly oriented crystallites, as suggested by the multiple isotropic scattering rings in its GIWAXS pattern (Figure 2e). The horizontal line cut of the powder GIWAXS has the same pattern as that of the powder XRD (Figure S17 in ESI), which validates that GIWAXS is a sensible technique in probing the solid state ordering within COFs. A comparison of the horizontal line cuts of the thin film and powder COF samples reveals the same (110) and (220) scattering peaks at 0.28 Å<sup>-1</sup> and 0.55 Å<sup>-1</sup>, suggesting the similar framework in both samples. Meanwhile, the (100) peak at 0.20 Å<sup>-1</sup> and (210) peak 0.44 Å<sup>-1</sup> disappear and a new (200) peak at 0.38 Å<sup>-1</sup> emerges in the thin film scattering pattern, which were attributed to preferential orientation of COF in the thin film.



**Figure 3.** The *I-V* curves of the TTF-COF thin film devices (a) before (black) and after exposure to I<sub>2</sub> for 24 hours (red), and (c) before (black) and after exposure to TCNQ for 24 hours (red). Time dependent conductivity changes of TTF-COF thin films upon exposure to (b) I<sub>2</sub> and (d) TCNQ. The arrows in (b) and (d) indicate the time of the thin films being removed from doping environments and kept in open air.

Conductivity measurements were carried out on TTF-COF thin films grown on Si/SiO<sub>2</sub> (300 nm) substrate with pre-fabricated Au/Cr electrodes that were 3 mm long, 50 nm thick and 125 μm apart (Figure S21). Current-voltage curves (*I-V*) obtained on such thin film devices exhibit (Figure 3a, black curve) a linear *I-V* response, corresponding to a conductivity of 1.2 × 10<sup>-4</sup> S/m. This is in contrast to the *I-V* characteristics of the analogue compound that is insulating (Figure S22). Exposure of the thin film to I<sub>2</sub> vapor in a closed chamber results in significant increase of electrical conductivity. A time-dependent study reveals (Figure 3b) that the conductivity

reaches a maximum of 0.28 S/m and saturates after exposure to I<sub>2</sub> for 24 hours. This doping is reversed to some extent, as the conductivity decreases to 1.0 × 10<sup>-3</sup> S/m after the film is removed from the I<sub>2</sub> chamber and left in open air over the course of 48 hours.

The TTF-COF thin film on transparent glass substrates allows detailed optical absorption studies in transmission mode. The UV-vis-near IR (NIR) spectra of TTF-COF thin films reveal (Figure 4a) a strong peak at 378 nm and a low intensity broad intramolecular charge-transfer band<sup>22</sup> centered at 550 nm, which are red shifted by 45 nm and 90 nm, respectively, when compared to these of the analogue **2** (Figure S23). Such bathochromic shifts are consistent with the formation of extended π systems in the COF films. Notably, a broad, low intensity peak in the NIR region is present only in the spectra of TTF-COF thin films but not the analogue **2**. This is a diagnostic NIR absorption band for the mixed-valence TTF species formed between TTF and TTF radical cation,<sup>23</sup> suggesting that there are significant free radicals delocalizing across the stacked sheets, which are responsible for the relatively high conductivity in the pristine TTF-COF.

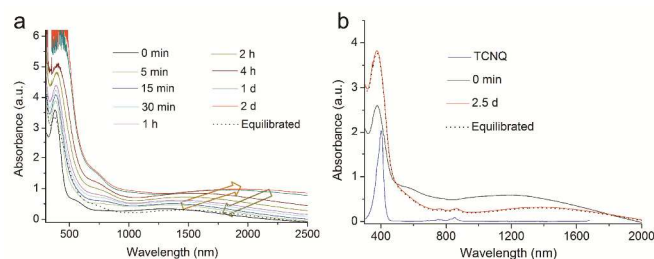


**Figure 4.** (a) UV-vis-NIR spectra of the TTF-COF thin film that is exposed to I<sub>2</sub> vapor for various amount of time (colored curves), (b) UV-vis-NIR spectra of TCNQ (blue, in THF), the TTF-COF thin film before (black) and after exposure (red) to a TCNQ solution in CH<sub>2</sub>Cl<sub>2</sub>. The dotted curves are the absorption of doped films after leaving in open air for 24 hours.

The UV-vis-NIR spectra of the TTF-COF thin film at different times of I<sub>2</sub> doping reveals (Figure 4a) that the NIR peak exhibits a progressive red shift from 1200 nm to more than 2000 nm over the course of I<sub>2</sub> exposure. These spectroscopic changes, which correlate with the conductivity enhancement, clearly indicate the formation of more delocalized mixed-valence TTF species. After leaving the doped film in open air for 24 hours, the NIR peak undergoes a hypochromic shift to a position close to that in the spectrum of the pristine sample, suggesting that the formation of such doped state is reversible to some extent. This reverse spectroscopic shift corroborates with the decrease of the film conductivity and is attributed to the volatility of I<sub>2</sub>. The TTF-COF film was also doped with nonvolatile TCNQ by immersion in its CH<sub>2</sub>Cl<sub>2</sub> solution. Bathochromic shift of the NIR peak (Figure 4b) as well as conductivity enhancement (Figure 3c) are again observed albeit with a lower magnitude. The UV-vis-NIR spectrum of the TCNQ-exposed film indicates a 200 nm red shift of the diagnostic NIR band, which is stable and remains unchanged in the air over the course of 24 hours. Such spectroscopic changes are once again consistent with the

conductivity measurement — after the conductivity reaches equilibrium, it remains similar after the TTF-COF film is removed from the TCNQ solution and kept in open air (Figure 3d).

Electron paramagnetic resonance (EPR) studies of the solid compounds further confirmed the effectiveness of chemical doping. A weak signal in the EPR spectrum of the pristine TTF-COF indicates the presence of very small amount of paramagnetic TTF<sup>•+</sup>, which corresponds to weakly doped TTF in as-synthesized COF and is consistent with the absorption spectrum (Figure 5). The paramagnetic intensity increased by approximately one and three orders of magnitude after TCNQ and I<sub>2</sub> doping, respectively, clearly validating the increased concentration of TTF<sup>•+</sup> and different degrees of doping. In addition, doping with TCNQ gives rise to a hyperfine structure associated with formation of TCNQ<sup>•-</sup> and consequent nitrogen nuclear magnetic coupling with peak splitting. Simulated results for the TTF-COF sample indicate the existence of two types of paramagnetic centers, with a main component of  $g=2.0065$  (97%) and a minor component (3%) with  $g=2.003$  (Figure 6 and Table S3). After doping with TCNQ, the EPR spectrum shows hyperfine splitting induced by the two <sup>14</sup>N from TCNQ structure, in addition to the  $g$  value from TTF<sup>•+</sup>. The  $g$ -values for this system are  $g_{zz} = 2.0026$ ,  $g_{xx} = 2.0065$ , and  $g_{yy} = 2.0086$ , which are consistent with literature results for TTF-TCNQ single crystal.<sup>24</sup> Similar to previously reported EPR measurements of polymer based-TTF,<sup>25</sup> simulated results of I<sub>2</sub>-doped TTF-COF show that the  $g$ -value is 2.0065 and equal to the average  $g$ -value for TTF-COF, with increased spin-spin interaction upon doping.

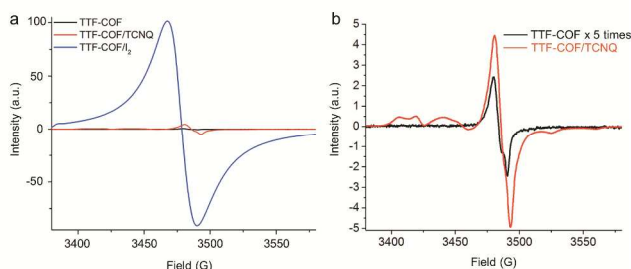


**Figure 5.** (a) The X-band EPR spectra of pristine (black), TCNQ doped (red), and I<sub>2</sub> doped TTF-COF (blue), and (b) the blowup of the signals of pristine and TCNQ-doped TTF-COF.

Similar to these observed in organogels<sup>26</sup> and in mechanically interlocked [3]catenanes,<sup>27</sup> the close proximity of pre-organized TTF units within COF is a prerequisite for the formation of such mixed-valence TTF species. In the control experiments when a thin film of the analogue compound **2** was subjected to doping, no NIR peaks were observed, highlighting the importance of columnar preorganization (Figure S24). While the corresponding FTIR spectra indicate doping-induced spectroscopic shifts (Figure S9 and S12), PXRD studies suggest that the crystallinity of the TTF-COF is maintained after doping (Figure S18). Structure-enabled properties are thus manifested in TTF-COF: the porous network structure permits dopant

diffusion for effective charge transfer, while the columnar stacking of TTF units enables delocalization of radical cations to generate more conductive mixed-valence species. The different doping levels could be ascribed to the mobility of the dopants within the pores as well as different degree of charge-transfer.

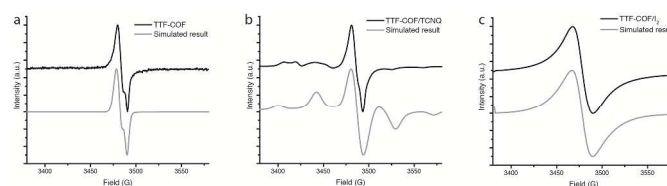


**Figure 6.** Experimental and simulated EPR spectra of (a) TTF-COF, (b) TTF-doped with TCNQ and (c) TTF-COF doped with I<sub>2</sub>.

## Conclusions

In summary, we report the synthesis and full characterization of a novel class of conductive 2D COF material, and its tunable electrical conductivity upon doping of the thin films grown on substrates. Different levels of doping are realized, resulting in high conductivities up to 0.28 S/m. The conductivity changes are correlated with diagnostic signatures in UV-vis-NIR and EPR spectra, pointing to effective radical delocalization within mixed-valence TTF stacks. It is conceivable that bicontinuous channels can be further optimized when different chemical linkage or spacers are employed. The present study thus opens the door to a more informed search for new electronic organic materials that combine the features of porous framework structure, convenient thin film formation, and tunable electrical conductivity.

## Experimental section

### Materials and Methods

The synthetic route is outlined in Scheme 1. TTF tetrabenzaldehyde<sup>21</sup> and the “monomeric” analogue compound tetraimino-TTF<sup>28</sup> were synthesized according to literature procedures. Other materials were reagent grade obtained from Aldrich and used without further purification; Dry solvents were collected from solvent purification system (JC Meyer Solvent Systems). Prepatterned ITO-coated glass substrates were purchased from Thin Film Devices Inc. 4” n-doped (Arsenic) Silicon Wafers with a thermally grown 300 nm oxide layer were obtained from Silicon Quest International. Thin-layer chromatography (TLC) was carried out using aluminum sheets, precoated with silica gel 60F (Merck 5554). The plates were inspected by UV-light. Melting points were measured by using an Electrothermal MEL-TEMP 3.0 apparatus and are uncorrected. Elemental analyses for C, H, N were performed on a Perkin Elmer 2400 Series II combustion analyzer. Grazing incidence wide angle X-ray scattering (GIWAXS) was conducted at Beamline 7.3.3 at the Advanced Light Source (ALS), Lawrence Berkeley National Laboratory, using an approximately 0.5 mm wide 10 keV X-ray beam. Electron

paramagnetic resonance (EPR) spectra were acquired using a Bruker ELEXSYS-II Brker spectrometer, equipped with a SuperX FT-EPR bridge and a 4102ST universal resonator, at the X-band (~9.8 G) at room temperature under air. Modulation frequency of 100 KHz, modulation amplitude of 5 G, and microwave attenuation of 2 db were employed to ensure the peak resolution and maximum intensity.

**Single Crystal Measurement.** Suitable single crystals of compounds 1 and 2 were selected under an optical microscope and quickly coated with epoxy before being mounted on a glass fiber for data collection. Data for them were collected on a Bruker APEX II CCD diffractometer equipped with a silicon 111 monochromator ( $T = 100$  K,  $k = 0.7749$  Å) on Station 11.3.1 at the ALS using synchrotron radiation. Structure solutions were solved by direct methods<sup>29</sup> and refined with the full-matrix least-squares methods on F2.<sup>29</sup> All non-hydrogen atoms were refined anisotropically, and all the hydrogen atom positions were fixed geometrically at calculated distances and allowed to ride on the parent atoms. Details of the crystal parameters, data collections, and refinements are summarized in Table S1. Crystallographic information files (CIFs) were deposited in Cambridge structural database, with Cambridge Crystallographic Data Center (CCDC) numbers 1001673-1001674 for compounds 1–2, respectively.

**Powder X-ray Diffraction Data Collection.** Powder X-ray diffraction (PXRD) was measured on a Bruker Gadds-8 diffractometer with a Cu-K $\alpha$  source operating at 40 kV and 20 mA. Powder X-ray diffraction data were collected using a Bruker D8-advance  $\theta$ - $\theta$  diffractometer in parallel beam geometry employing Cu K $\alpha$  line focused radiation at 1600 W (40 kV, 40 mA) power and equipped with a position sensitive detector with at 6.0 mm radiation entrance slit. Samples were mounted on zero background sample holders by dropping powders from a wide-blade spatula and then leveling the sample with a razor blade. For the THF exchanged sample, an air-tight sample holder was employed to avoid solvent evaporation during the data acquisition. The best counting statistics were achieved by collecting samples using a 0.02° 2 $\theta$  step scan from 2 – 50° with exposure time of 5 s per step. The Pawley PXRD refinement was performed using the Reflex module in the Materials Studio 5.0, in which a Pseudo-Voigt profile function was used for the profile fitting (peak broadening, peak asymmetry, and zero shift error were taken into account). Unit cell and sample parameter were refine simultaneously.

**Device Fabrication and Testing.** Silicon substrates were cut into 16 x 8 mm<sup>2</sup> pieces, and were then cleaned at 40 °C in soap water, DI water, acetone, and isopropanol under subsequent sonication before being dried in an oven at 130 °C for at least one hour. The substrates were then transferred to a thermal evaporator in a nitrogen glovebox where 45 nm of Au was evaporated on top of a 5 nm Cr adhesion layer through a shadow mask, to give a channel width and length of 3 mm and 125  $\mu$ m, respectively. After the COF film was grown upon the substrate as described below, the I-V responses were measured by two-probe measurement using a model CPX-HF Lakeshore

Probe Station and an Agilent 4155C Semiconductor parameter Analyzer at room temperature and pressure.

**Synthesis of TTF tetrabenzaldehyde (1).** A 50 mL two-neck round bottom flask was charged with Cs<sub>2</sub>CO<sub>3</sub> (1.95 g, 6.0 mmol), Pd(OAc)<sub>2</sub> (78.6 mg, 0.35 mmol) and PtBu<sub>3</sub>•HBF<sub>4</sub> (267 mg, 0.90 mmol), and was subjected to three cycles of evacuation and refilling with nitrogen. Anhydrous THF (8.0 mL) was added and the suspension was heated at 76 °C for 15 min under stirring. Then, a solution of tetrathiafulvalene (204 mg, 1.0 mmol) and 4-bromobenzaldehyde (1.11 g, 6.0 mmol) in anhydrous THF (8.0 mL) was added. The reaction mixture was refluxed for 15 h and then cooled to room temperature. The solid was filtered off and washed with THF thoroughly, and the combined filtrate was concentrated under reduced pressure. The resulting residue was washed with hexane (150 mL) and subjected to column chromatography (silica gel, chloroform 100%). The compound was further purified by recrystallization from chloroform/cyclohexane to yield **1** as dark red needle crystals (155 mg, 25% yield). <sup>1</sup>H NMR (CDCl<sub>3</sub>, 298 K, 500 MHz):  $\delta$  = 7.40 (d,  $J$  = 8.0 Hz, 8H), 7.80 (d,  $J$  = 8.5 Hz, 8H), 10.00 (s, 4H); <sup>13</sup>C NMR (CDCl<sub>3</sub>, 298 K, 125 MHz): 108.8, 129.7, 130.1, 130.3, 136.2, 138.0, 191.1. M.P.: >330 °C (dec). MS (MALDI-TOF): [M + H]<sup>+</sup> calcd for C<sub>34</sub>H<sub>20</sub>O<sub>4</sub>S<sub>4</sub>: 620.02; found: 620.24.

**Synthesis of the analogue compound tetraimino-TTF (2).** A mixture of **1** (19.2 mg, 0.031 mmol) and aniline (14.4 mg, 0.155 mmol) in a round bottle flask was dissolved in dry toluene (8.0 mL). The flask was connected to a Dean–Stark apparatus and stirred at 130 °C for 5 h. The reaction mixture was cooled to room temperature and the dark red crystals of the model compound were obtained by filtration and dried under vacuum (26.8 mg, 94% yield). <sup>1</sup>H NMR (CDCl<sub>3</sub>, 298 K, 500 MHz):  $\delta$  = 7.23 (dd,  $J$  = 8.5 Hz, 1.0 Hz, 8H), 7.25–7.28 (m, 4H), 7.38 (dd,  $J$  = 6.5 Hz, 1.5 Hz, 8H), 7.41–7.44 (m, 8H), 7.83 (dd,  $J$  = 6.5 Hz, 1.5 Hz, 8H), 8.44 (s, 4H); <sup>13</sup>C NMR (CDCl<sub>3</sub>, 298 K, 125 MHz): 108.7, 120.9, 126.2, 129.1, 129.2, 129.5, 129.8, 135.3, 136.3, 151.7, 159.2. M.P.: >330 °C (dec). MS (MALDI-TOF): [M + H]<sup>+</sup> calcd for C<sub>58</sub>H<sub>40</sub>N<sub>4</sub>S<sub>4</sub>: 920.21; found: 920.31.

**Synthesis of TTF-COF powder and thin films.** A 10 mL microwave reaction vial was charged with **1** (24.8 mg, 0.040 mmol), **1**, 4-diaminobenzene (8.64 mg, 0.080 mmol), anhydrous 1,4-dioxane (2 mL), mesitylene (2 mL) and 3 M acetic acid (0.4 mL). The resulting mixture was sonicated for 15 minutes and then was bubbled with nitrogen for 15 minutes under stirring. The vial was quickly sealed by a Teflon cap and heated at 120 °C for 3 days. After cooling to room temperature, the deep purple precipitate was collected by vacuum filtration, washed with anhydrous THF for several times and anhydrous acetone once, before being dried under vacuum at 120 °C overnight to yield a deep purple solid of TTF-COF (16.7 mg, 52% yield). Elemental analysis: Calcd. for C<sub>46</sub>H<sub>28</sub>N<sub>4</sub>S<sub>2</sub>: C, 72.20; H, 3.69; N, 7.32%. Found: C, 72.03; H, 3.73; N, 7.59%. For thin film growth, a piece of corresponding substrate (ITO glass, Silicon wafer with or without prepatterned Au electrodes) was placed in the reaction vial containing the above mixtures.

After the reaction, the substrate was retrieved, washed thoroughly with organic solvents, and dried before testing.

## Acknowledgements

This work was performed at the Molecular Foundry, with EPR measurements conducted at the Joint Center for Artificial Photosynthesis, a DOE Energy Innovation Hub. They are supported through the Office of Science, Office of Basic Energy Sciences, of the U.S. Department of Energy, under Contract No. DE-AC02-05CH11231 and Award No. DE-SC0004993, respectively. B.H. and Y.L. are supported by the Inorganic-Organic Nanocomposites program under the same contract number. S.C. is grateful to the Chinese Scholarship Council for a fellowship. A.B.P. is supported by a DOE SULI internship. W.Z. acknowledges the support from NSF China (Grant No. 21171059). Y.Z. and O.M.Y. acknowledge the support from BASF SE (Ludwigshafen, Germany) and DOE ARPA-E (DE-AR0000251). We thank Dr. Simon J. Teat (Beam 11.3.1) and Dr. Chenhui Zhu (Beam 7.3.3) of Advanced Light Source for synchrotron X-ray studies.

## Notes and references

<sup>a</sup> The Molecular Foundry, Lawrence Berkeley National Laboratory, Berkeley, California 94720, United States, E-mail: yliu@lbl.gov

<sup>b</sup> School of Chemistry and Environment, South China Normal University, Guangzhou 510006, P. R. China, E-mail: wgzhang@snu.edu.cn

<sup>c</sup> Department of Chemistry, University of California–Berkeley, and Kavli Energy NanoSciences Institute at Berkeley, Berkeley, California 94720, United States

<sup>d</sup> Joint Center for Artificial Photosynthesis, Lawrence Berkeley National Laboratory, Berkeley, California 94720, United States

<sup>e</sup> Material Sciences Division, Lawrence Berkeley National Laboratory, Berkeley, California 94720, United States

<sup>f</sup> Chemical Sciences Division, Lawrence Berkeley National Laboratory, Berkeley, California 94720, United States

<sup>g</sup> Physical Biosciences Division, Lawrence Berkeley National Laboratory, Berkeley, California 94720, United States

† These authors contributed equally.

Electronic Supplementary Information (ESI) available: IR spectra, solid-state NMR spectrum, SEM, PXRD analysis and coordinates of crystal structure model, nitrogen adsorption isotherm, TGA trace, conductivity measurement, UV-vis-NIR spectra, cif files. See DOI: 10.1039/b000000x/

- (a) M. Bendikov, F. Wudl and D. F. Perepichka, *Chem. Rev.*, 2004, **104**, 4891-4946; (b) D. Canevet, M. Salle, G. Zhang, D. Zhang and D. Zhu, *Chem. Commun.*, 2009, DOI: 10.1039/B818607N, 2245-2269.
- (a) V. Coropceanu, J. Cornil, D. A. da Silva Filho, Y. Olivier, R. Silbey and J.-L. Brédas, *Chem. Rev.*, 2007, **107**, 926-952; (b) B. C. Thompson and J. M. J. Frechet, *Angew. Chem. Int. Ed.*, 2008, **47**, 58-77.
- S. Savagatrup, A. D. Printz, T. F. O'Connor, A. V. Zaretski and D. J. Lipomi, *Chem. Mater.*, 2014, **26**, 3028-3041.
- (a) J. W. Colson and W. R. Dichtel, *Nat. Chem.*, 2013, **5**, 453-465; (b) A. P. Côté, A. I. Benin, N. W. Ockwig, M. O'Keeffe, A. J. Matzger and O. M. Yaghi, *Science*, 2005, **310**, 1166-1170; (c) X. Feng, X. Ding and D. Jiang, *Chem. Soc. Rev.*, 2012, **41**, 6010-6022; (d) S. Kandambeth, A. Mallick, B. Lukose, M. V. Mane, T. Heine and R. Banerjee, *J. Am. Chem. Soc.*, 2012, **134**, 19524-19527.
- M. Dogru and T. Bein, *Chem. Commun.*, 2014, **50**, 5531-5546.
- (a) G. H. V. Bertrand, V. K. Michaelis, T.-C. Ong, R. G. Griffin and M. Dincă, *Proc. Natl. Acad. Sci.*, 2013, **110**, 4923-4928; (b) M. Dogru, M. Handloser, F. Auras, T. Kunz, D. Medina, A. Hartschuh, P. Knochel and T. Bein, *Angew. Chem. Int. Ed.*, 2013, **52**, 2920-2924.
- (a) S. Wan, J. Guo, J. Kim, H. Ihee and D. Jiang, *Angew. Chem. Int. Ed.*, 2009, **48**, 5439-5442; (b) S. Wan, J. Guo, J. Kim, H. Ihee and D. Jiang, *Angew. Chem. Int. Ed.*, 2008, **47**, 8826-8830.
- (a) X. Ding, L. Chen, Y. Honsho, X. Feng, O. Saengsawang, J. Guo, A. Saeki, S. Seki, S. Irle, S. Nagase, V. Parasuk and D. Jiang, *J. Am. Chem. Soc.*, 2011, **133**, 14510-14513; (b) X. Ding, J. Guo, X. Feng, Y. Honsho, J. Guo, S. Seki, P. Maitarad, A. Saeki, S. Nagase and D. Jiang, *Angew. Chem. Int. Ed.*, 2011, **50**, 1289-1293; (c) E. L. Spitler and W. R. Dichtel, *Nat. Chem.*, 2010, **2**, 672-677.
- S. Wan, F. Gándara, A. Asano, H. Furukawa, A. Saeki, S. K. Dey, L. Liao, M. W. Ambrogio, Y. Y. Botros, X. Duan, S. Seki, J. F. Stoddart and O. M. Yaghi, *Chem. Mater.*, 2011, **23**, 4094-4097.
- A. Nagai, X. Chen, X. Feng, X. Ding, Z. Guo and D. Jiang, *Angew. Chem. Int. Ed.*, 2013, **52**, 3770-3774.
- (a) S. Jin, X. Ding, X. Feng, M. Supur, K. Furukawa, S. Takahashi, M. Addicoat, M. E. El-Khouly, T. Nakamura, S. Irle, S. Fukuzumi, A. Nagai and D. Jiang, *Angew. Chem. Int. Ed.*, 2013, **52**, 2017-2021; (b) E. L. Spitler, J. W. Colson, F. J. Uribe-Romo, A. R. Woll, M. R. Giovino, A. Saldivar and W. R. Dichtel, *Angew. Chem. Int. Ed.*, 2012, **51**, 2623-2627.
- X. Feng, L. Chen, Y. Honsho, O. Saengsawang, L. Liu, L. Wang, A. Saeki, S. Irle, S. Seki, Y. Dong and D. Jiang, *Adv. Mater.*, 2012, **24**, 3026-3031.
- C. R. DeBlase, K. E. Silberstein, T.-T. Truong, H. D. Abruña and W. R. Dichtel, *J. Am. Chem. Soc.*, 2013, **135**, 16821-16824.
- J. Mei, Y. Diao, A. L. Appleton, L. Fang and Z. Bao, *J. Am. Chem. Soc.*, 2013, **135**, 6724-6746.
- (a) J. W. Colson, A. R. Woll, A. Mukherjee, M. P. Levendorf, E. L. Spitler, V. B. Shields, M. G. Spencer, J. Park and W. R. Dichtel, *Science*, 2011, **332**, 228-231; (b) D. D. Medina, V. Werner, F. Auras, R. Tautz, M. Dogru, J. Schuster, S. Linke, M. Döblinger, J. Feldmann, P. Knochel and T. Bein, *ACS Nano*, 2014, **8**, 4042-4052.
- X.-H. Liu, C.-Z. Guan, S.-Y. Ding, W. Wang, H.-J. Yan, D. Wang and L.-J. Wan, *J. Am. Chem. Soc.*, 2013, **135**, 10470-10474.
- A. A. Talin, A. Centrone, A. C. Ford, M. E. Foster, V. Stavila, P. Haney, R. A. Kinney, V. Szalai, F. El Gabaly, H. P. Yoon, F. Léonard and M. D. Allendorf, *Science*, 2014, **343**, 66-69.
- (a) F. Wudl, D. Wobschall and E. J. Hufnagel, *J. Am. Chem. Soc.*, 1972, **94**, 670-672; (b) J. Ferraris, D. O. Cowan, V. Walatka and J. H. Perlstein, *J. Am. Chem. Soc.*, 1973, **95**, 948-949; (c) J. Xiao, Z. Yin, H. Li, Q. Zhang, F. Boey, H. Zhang and Q. Zhang, *J. Am. Chem. Soc.*, 2010, **132**, 6926-6928.
- (a) T. C. Narayan, T. Miyakai, S. Seki and M. Dincă, *J. Am. Chem. Soc.*, 2012, **134**, 12932-12935; (b) C. F. Leong, B. Chan, T. B. Faust and D. M. D'Alessandro, *Chem. Sci.*, 2014, DOI: 10.1039/C4SC01551G.

20. During the preparation of this manuscript, we notice that Jiang et al. independently reported the formation of a closely-related TTF-COF in its powder form. See DOI: 10.1002/chem.201402844.
21. Y. Mitamura, H. Yorimitsu, K. Oshima and A. Osuka, *Chem. Sci.*, 2011, **2**, 2017-2021.
22. These low-energy absorptions were caused by intramolecular charge transfer from TTF to imino moieties. Similar behavior was observed in other TTF- $\pi$ -acceptor derivatives. See reference 20.
23. R. Bozio, I. Zanon, A. Girlando and C. Pecile, *J. Chem. Phys.*, 1979, **71**, 2282-2293.
24. Y. Tomkiewicz, B. A. Scott, L. J. Tao and R. S. Title, *Phys. Rev. Lett.*, 1974, **32**, 1363-1366.
25. V. I. Krinichnyi, N.N. Denisov, H.-K. Roth, E. Fanghänel and K. Lüders, *Polym. Sci. A*, 1998, **40**, 1259-1267.
26. (a) T. Kitahara, M. Shirakawa, S.-i. Kawano, U. Beginn, N. Fujita and S. Shinkai, *J. Am. Chem. Soc.*, 2005, **127**, 14980-14981; (b) T. Kitamura, S. Nakaso, N. Mizoshita, Y. Tochigi, T. Shimomura, M. Moriyama, K. Ito and T. Kato, *J. Am. Chem. Soc.*, 2005, **127**, 14769-14775.
27. J. M. Spruell, A. Coskun, D. C. Friedman, R. S. Forgan, A. A. Sarjeant, A. Trabolsi, A. C. Fahrenbach, G. Barin, W. F. Paxton, S. K. Dey, M. A. Olson, D. Benítez, E. Tkatchouk, M. T. Colvin, R. Carmielli, S. T. Caldwell, G. M. Rosair, S. G. Hewage, F. Duclairoir, J. L. Seymour, A. M. Z. Slawin, W. A. Goddard, M. R. Wasielewski, G. Cooke and J. F. Stoddart, *Nat. Chem.*, 2010, **2**, 870-879.
28. Y.-B. Zhang, J. Su, H. Furukawa, Y. Yun, F. Gándara, A. Duong, X. Zou and O. M. Yaghi, *J. Am. Chem. Soc.*, 2013, **135**, 16336-16339.
29. G. Sheldrick, *Acta Crystallographica Section A*, 2008, **64**, 112-122.